R. F. Broom
R. Jaggi
Th. O. Mohr
A. Oosenbrug

Effect of Process Variables on Electrical Properties of Pb-Alloy Josephson Junctions

Our studies on the effect of process variables on the electrical properties of Josephson tunnel junctions were directed toward optimization of the process for cryogenic memory applications, for which special importance is placed on the dc Josephson current density j_1*, its stability and reproducibility, and the junction quality. Variables studied included rf voltage, oxygen plasma pressure, the presence of oxygen during deposition of the counter electrode, the composition and surface state of the base electrode, junction geometry, radial position on the wafer, and storage and annealing conditions. Various process adjustments were made in order to obtain acceptable device characteristics. For example, good tunnel characteristics could be obtained using Pb-Au-In alloys if In concentrations >8 wt% (for a fixed 3% Au concentration) were used in the base electrode. High pressure and low rf voltage during oxidation were preferable, since these conditions led to low annealing factors. We were also able to adjust* j_1 *locally by irradiation with high-energy (>5 keV) electrons.*

Introduction

The advantages of a high-performance, low-power cryogenic memory have been demonstrated with a single-flux-quantum (SFQ) memory cell [1-2]. The demonstration vehicle based on this cell contains the critical elements of a main memory in Josephson technology [3]. The techniques used to fabricate the memory cross-sectional model were adapted from ones already in use [4-7].

The effects of varying process parameters on the electrical properties of Josephson tunnel junctions are described in this paper. Two categories can be distinguished: effects on the Josephson current density and effects on the single-particle tunnel characteristics.

The composition, thickness, and purpose of the various layers used are slightly different from those discussed by Greiner *et al.* in an accompanying paper in this issue [8]. The basic differences are the absence of the I_{1c}, C, and I_{2b} layers; base-electrode (M_2) and control-line (M_4) compositions of Pb-In(12 wt%)-Au(3 wt%); and a counter-electrode (M_3) composition of Pb-Au(2.5 wt%)-Pb(36 wt%).

All the metal and insulating layers, except for the M_1 ground plane (subtractively wet-etched) are patterned by using lift-off techniques. See Refs. [8-9] for a detailed description of the profile requirements and patterning process.

The high-vacuum systems used for deposition of junction electrodes and control lines and for rf oxidation of the tunnel barrier [10] were equipped for simultaneous processing of multiple wafers. The evaporation sources for Pb, In, and Au were tungsten crucibles with vitreous carbon inserts, thermally heated by electron bombardment. A schematic drawing of the system is shown in Fig. 1.

Current density dependences

Josephson current density j_1 is an important parameter in electrical device performance. To satisfy circuit requirements j_1 should be within ±10% of a prescribed value. This section outlines key process variables and their effects on j_1. In addition, methods are described to adjust j_1 with post-fabrication treatments.

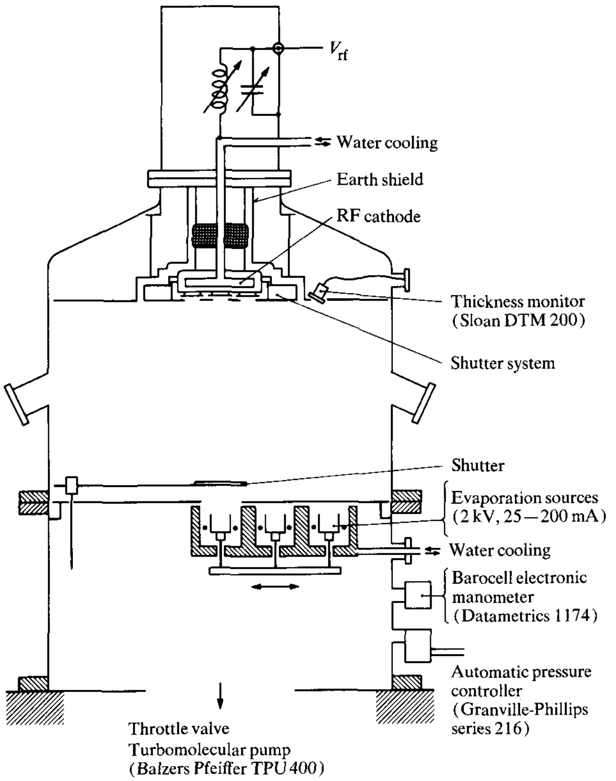

Figure 1 Schematic diagram of the vacuum system.

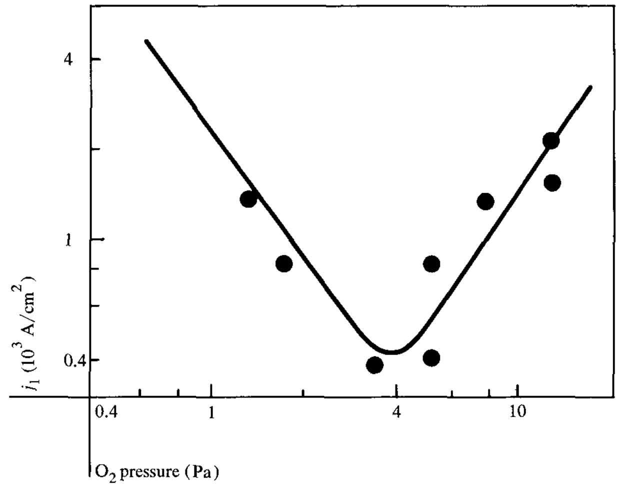

Figure 2 Dependence of j_1 on oxygen plasma pressure for V_{rf} = 230 V.

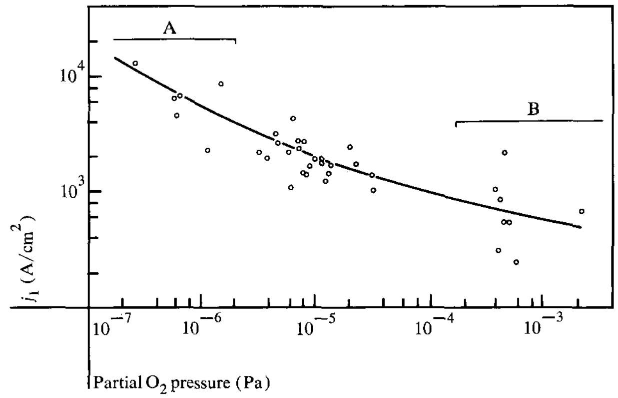

Figure 3 Dependence of j_1 on partial pressure of oxygen in the system during deposition of the first monolayers of M_3. The range A represents data for M_3 deposition after Ar or N_2 rf cleaning; range B is for M_3 deposition in an oxygen atmosphere.

- *RF voltage*

During the formation of the tunnel barrier two mechanisms are competing: oxide growth and oxide sputter etching. After a 40-min rf oxidation these mechanisms are in equilibrium. The resulting tunnel-barrier-layer thickness, which determines j_1, strongly depends on plasma energy. At a constant oxygen plasma pressure there is an inverse proportionality, with j_1 decreasing with increasing rf voltage (all voltages are peak-to-peak). Higher plasma energies result in thicker barrier layers, indicating that oxidation exceeds sputter etching.

The high sensitivity of j_1 to changes in the tunnel barrier explains why the rf voltage dependence is different in each vacuum system, since the geometrical arrangement influences properties of the plasma and backscattering of material during rf oxidation.

- *Pressure of oxygen plasma*

Figure 2 shows the dependence of j_1 on oxygen plasma pressure at fixed rf voltage. At low but increasing pressures (≈0.5 Pa), j_1 first decreases because of the larger number of ions available for oxidation. Above the minimum (≈4 Pa), j_1 is dependent on several competing processes: charge neutralization caused by collisions of positive and negative oxygen ions, energy losses and reduction in the primary sputtering rate due to collisions of ions with molecules, and increased backscattering at higher pressures.

- *Influence of oxygen during deposition of counter electrode (M_3)*

In addition to the plasma-grown and backscattered barrier layer, some oxide is formed at the interface between the barrier and counter electrode by reaction of Pb with adsorbed oxygen. The amount of adsorbed oxygen is primarily determined by the background conditions prior to M_3 deposition. Figure 3 shows the dependence of the Jo-

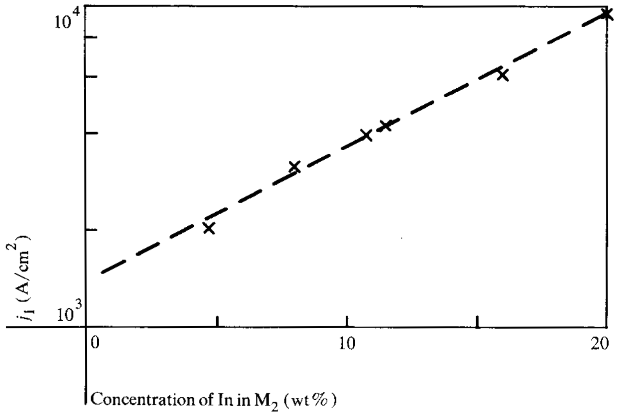

Figure 4 Dependence of j_1 on the indium concentration in the base electrode (M_2).

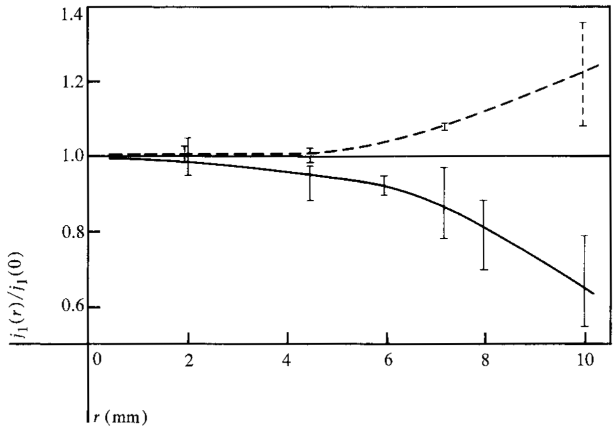

Figure 5 Systematic variation of j_1 over a 32-mm wafer for rf oxidation at O_2 pressures of 0.4 (---) and 0.8 Pa (—); r is the distance of the chip from the center of the wafer (defined as $r = 0$).

sephson current density on the partial oxygen pressure in the system measured during the deposition of the first monolayers of Pb of the Pb-Au-Pb counter electrode.

The partial pressure of oxygen increases during deposition due to release of oxygen atoms adsorbed on the parts of the system. This increase can be related to the source temperature, the bell-jar temperature, the amount of metal evaporant on the system parts, and in particular to the history of the system. Rf-system cleaning with Ar or N_2 after tunnel-barrier formation results in a hardly detectable amount of oxygen desorbed during M_3 deposition, and a much higher j_1. On the other hand, j_1 is drastically reduced if M_3 deposition occurs in an increased background of oxygen.

- *Base-electrode (M_2) composition and surface state*

The composition of the base electrode M_2 should be carefully controlled to achieve acceptable run-to-run reproducibility in j_1. The influence on j_1 of a varying In concentration in M_2 is shown in Fig. 4. The Au content was kept constant at 3 wt%. It can be seen that j_1 increases with the In concentration. The more In available in M_2, the higher its concentration will be at the top surface. This leads to more In_2O_3 in the tunnel barrier layer and thus, increased current density [11].

During resist processing the surface of the M_2 layer is exposed to atmosphere and to chemical solutions. Resulting surface reactions and gas adsorption cause irreproducible changes in the M_2 surface, as evidenced by ellipsometric measurements of M_2 layers before and after resist processing. The original readings could not be restored by rf cleaning in Ar. Junctions prepared on rf-argon-cleaned M_2 surfaces usually had a lower j_1 and a much larger spread σ in j_1 as compared to junctions prepared on untreated wafers. Apparently the rf cleaning of the alloy surface introduces local variations in surface composition.

No clear dependence of j_1 on resist development times was found; however, j_1 is increased considerably by extended washing of the M_2 layer in deionized water. An increase of ≈50% was found for a washing time of 210 s as compared to 90 s. During washing some Pb is etched off and dissolved in deionized water (as lead hydroxide). This leads to a higher In concentration at the M_2 surface and thus a j_1 increase.

- *Junction geometry*

Current density is influenced by junction geometry. It is lower for small-area junctions and levels off with increasing dimensions. This j_1 "size effect" is affected by the thickness of and the material used for I_{2a}, and becomes more pronounced with increasing thickness, suggesting that backscattering of insulating material from the steep I_{2a} edges to the periphery of the junction during rf oxidation is an important factor in understanding the size effect. The observation that long narrow junctions exhibited lower j_1 values than square junctions of the same area is consistent with this model. A further possible explanation involves different charging of the oxide.

The differences observed in the area dependence of j_1 with the use of different I_{2a} materials probably result from variations in sputtering yield for these materials and/or from material-dependent changes in the local potential distribution at the wafer surface during rf oxidation. In an experiment where we compared the use of Nb, Si, Al_2O_3, Al, or In as thin layers on top of I_{2a} (SiO), Nb showed the smallest (1.08), and In the largest (1.30), size effect (expressed in j_1 ratios for 200-μm^2 and 30-μm^2 junctions).

Radial position on the wafer

Current density is nonuniform over the area of a wafer. With an rf oxidation at 0.8 Pa of O_2, j_1 is higher at the center of a 32-mm wafer than at the periphery, the difference being ≈25%. See Fig. 5, where r is the distance of the chip from the center of the wafer. The steepest decrease in j_1 is observed at the wafer periphery. The local variation in current density on a wafer can be reversed by a change in plasma pressure. For rf oxidation at 0.1 or 0.4 Pa, the lowest value of j_1 is found in the center of the wafer [$=j_1(0)$].

Factors which affect uniformity are the perturbation of the cathode potential by a static charge on the wafer [12] and backscattering of material from the cathode body [11].

Storage

Storage stability of j_1 was tested on interferometer structures [13] protected by 2 μm of SiO under four different conditions:

1. At room temperature in dry air of a desiccator.
2. At room temperature in vacuum better than 10^{-3} Pa.
3. At −24°C not protected from humidity.
4. At liquid-nitrogen temperature.

The results are shown for full-window junction interferometers (junction area defined by I_{2a}) in Fig. 6, where j_1(after storage)/j_1(initial), averaged over eighty interferometers, is plotted *versus* storage time. Best stability is found on samples stored in liquid nitrogen. The results are still reasonable for storage in vacuum and dry air, where only small changes in j_1 have been observed; however, the results from chips stored at −24°C in a humid atmosphere are unacceptable. The I_4 layer apparently does not prevent penetration of water vapor into the junction.

Annealing

Annealing changes the current density of Josephson devices. In Fig. 7, the annealing factor

$$\alpha = \frac{j_1\,(\text{after annealing})}{j_1\,(\text{before annealing})} \tag{1}$$

is plotted *versus* the oxygen pressure during rf oxidation. The four curves refer to different rf voltages and annealing times. In the low-pressure range, α is generally greater than unity and increases for higher rf voltages. At high pressure and low voltage, current density is reduced by annealing. The changes observed in j_1 indicate that the as-fabricated barrier layer is not in its equilibrium state. To explain the junction behavior during annealing at least two competing processes would have to occur, j_1 being increased by one and decreased by the other. Possible mechanisms invoke changes in oxide composition or crystal structure, densification of backsputtered oxide, or reaction of excess oxygen with the electrode material.

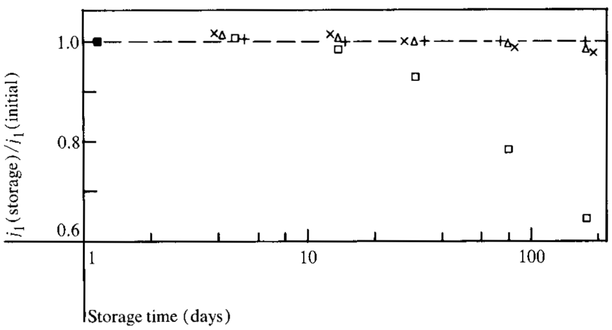

Figure 6 Storage behavior for full-window junction interferometers protected by 2 μm of SiO. Data points are for the following storage conditions: +, liquid N_2; Δ, vacuum; ×, desiccator; and □, −20°C.

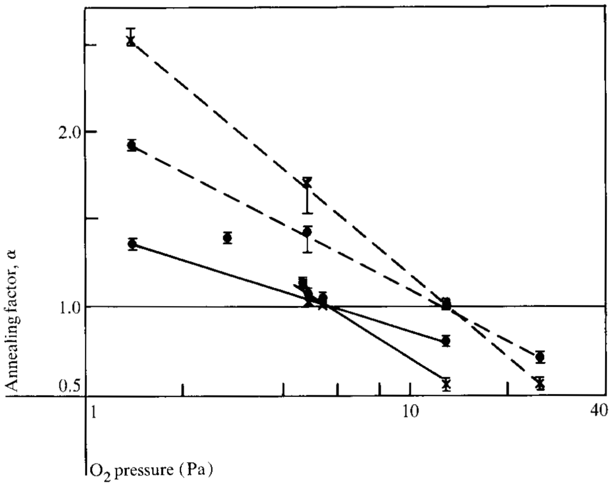

Figure 7 Annealing factor *versus* pressure during 40-min rf oxidation at 100 (—) and 200 V (---). Data points are for 80°C anneal for 1 (●) and 4 h (β).

The current density approaches a constant value with extended annealing time. Thus structures baked a number of times during resist processing are partially stabilized on completion.

Local adjustment of current density

The temperature treatment of completed devices can be used to make j_1 adjustments. The increase (or decrease) in

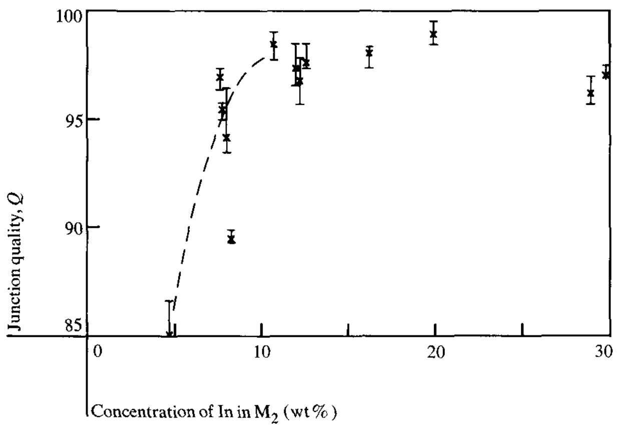

Figure 8 Junction quality Q *versus* concentration of indium in M_2.

j_1 is uniform over the chip or wafer area. A local adjustment of j_1 is possible by irradiating particular junctions with electrons with energies higher than 5 keV. The room-temperature resistance of these junctions decreases with increasing electron exposure. This is most likely due to the creation of disorder in the tunneling oxide by the high-energy electrons [14]. According to this resistance decrease, j_1 is increased. A j_1 increase of 50% is seen with an electron dosage of 10^{-1} C/cm^2 and an accelerating voltage of 30 kV. It is noteworthy that the electron irradiation treatment has no measurable effect on either the room-temperature storage or annealing behavior.

Single-particle tunnel-characteristic dependences

Two measures are used in the determination of the single-particle characteristics: the junction quality Q (measured below the half-gap voltage Δ/e) and V_m (an empirical measure of the single-particle current above Δ/e). The junction quality is given by

$$Q = 100\{1 - [R_{nn}I(1\ \text{mV}) - R_{nn}^{BCS}I_{BCS}(1\ \text{mV})]/1\ \text{mV}\}, \quad (2)$$

in which R_{nn} is the normal-state tunnel resistance, $I(1\ \text{mV})$ is the measured single-particle current at 1 mV, and $I_{BCS}(1\ \text{mV})$ is the tunnel current calculated from the Bardeen-Cooper-Schrieffer theory for an "ideal" junction at 4.2 K having a gap voltage $2\Delta/e = 2.5$ mV. [For $R_{nn}^{BCS} = 1\ \Omega$, $I_{BCS}(1\ \text{mV}) = 0.063$ mA.] Thus, Q represents the deviation from BCS theory. The value for V_m is given by $R_j i_1$, where R_j is defined as the linear resistance at 1.7 mV and i_1 is the maximum dc Josephson current ($j_1 \times$ area).

- *Dependence of Q on base-electrode (M_2) composition*

Figure 8 shows Q as a function of the In concentration in M_2. The degradation of Q at low-In concentrations is believed to be the result of the increasing influence of normal conducting material in M_2 when located close to the barrier. As In, Au, and Pb are deposited consecutively, it is to be expected that for higher In concentrations, less unreacted Au, $AuPb_2$, or $AuPb_3$ are found in the film because $AuIn_2$ is formed as a bottom layer [15, 16]. The excess In goes into solid solution with Pb and only small quantities of Au can diffuse into this solution. The junction quality is fairly constant for In concentrations >8-10%. For this reason the base-electrode (M_2) composition was fixed at Pb-In(12 wt%)-Au(3 wt%).

- *Dependence of V_m on the proximity of Au in the counter electrode (M_3)*

The Au concentration of 2.5 wt% is well below that required to convert the entire M_3 film to $AuPb_2$ or $AuPb_3$. These phases remain as thin films centered at the original location of the Au. Their influence on the tunnel characteristics will be a function of the separation between the Au/Pb phases and the oxide-M_3 interface. Indeed a considerable increase in V_m is seen (from 12 to 17 mV) for the Pb-Au(2.5 wt%)-Pb(36 wt%) M_3 composition compared to Pb(36 wt%)-Au(2.5 wt%)-Pb. Depositing more than 61 wt% Pb before Au deposition did not show further significant increase of V_m.

- *Dependence of V_m on current density*

It is reasonable to expect a decrease in V_m but little change in quality factor Q as j_1 is increased, because these quantities are measured at voltages above and below Δ/e, respectively. Qualitatively, such behavior is in fact observed.

The appropriate functional V_m dependence on j_1 should be of the form $V_m = V_{m0}/(A + Bj_1)$. However, many additional material variations such as alloy composition, free gold in grain boundaries, and the abruptness of the superconductor-oxide interface influence the first-order tunnel current and obscure the second-order effects by introducing relatively large random variations in V_m. For this reason, a simple linear approximation has been applied to the results. The overall downward trend of V_m with increasing j_1 is indeed found. A least-squares fit to the mean values of V_m for all junctions lying within intervals of 0.5 kA/cm^2 yields the relationship $V_m = 18.1 - 0.45j_1$, where j_1 is in kA/cm^2 and V_m in mV.

Summary

The main purpose of this paper is to describe how junction characteristics depend on process conditions. The results illustrate the measures taken to obtain acceptable device characteristics. The principal results are as follows. For a fixed Au concentration of 3 wt% in the base electrode (M_2), the In concentration must be >8 wt% to obtain good tunnel characteristics. Current density j_1 is a function of rf voltage and oxygen plasma pressure, but other preparation parameters must be considered. Some freedom of choice is available in adjusting these parameters for a given j_1 and a desired junction behavior. Finally, high pressure and low voltage lead to a low annealing factor and are therefore to be preferred.

Acknowledgments

We are most grateful to our coworkers K. Daetwyler, U. Deutsch, H. P. Dietrich, T. Forster, M. Gasser, W. Heuberger, L. Perriard, and G. Sasso for their contributions to the preparation of the devices used in this study. Thanks are also due coworkers H. Gschwind, H. Richard, and H. Weibel for carrying out the electrical measurements.

References

1. P. Guéret, *Appl. Phys. Lett.* **25,** 426 (1974); H. H. Zappe, *Appl. Phys. Lett.* **25,** 424 (1974).
2. P. Guéret, Th. O. Mohr, and P. Wolf, *IEEE Trans. Magnetics* **MAG-13,** 52 (1977).
3. P. Guéret, A. Moser, and P. Wolf, *IBM J. Res. Develop.* **24** (1980, this issue).
4. J. H. Greiner, *J. Appl. Phys.* **42,** 5151 (1971).
5. S. K. Lahiri and S. Basavaiah, *J. Appl. Phys.* **49,** 2880 (1978).
6. S. K. Lahiri, *Thin Solid Films* **41,** 209 (1977).
7. J. H. Greiner, S. Basavaiah, and I. Ames, *J. Vac. Sci. Technol.* **11,** 81 (1974).
8. M. Hatzakis, B. J. Canavello, and J. M. Shaw, *IBM J. Res. Develop.*, accepted for publication.
9. B. Canavello, M. Hatzakis, and J. M. Shaw, *IBM Tech. Disclosure Bull.* **19,** 4048 (1977).
10. Balzers AG, Model UTS 350, Balzers, Liechtenstein.
11. J. Baker, C. J. Kircher, and J. Matthews, *IBM J. Res. Develop.* **24** (1980, this issue).
12. P. Brosious, IBM Thomas J. Watson Research Center, Yorktown Heights, NY, private communication.
13. R. F. Broom and Th. O. Mohr, *J. Vac. Sci. Technol.* **15,** 1166 (1978).
14. E. Stoll and T. Schneider, *Solid State Commun.* **11,** 1327 (1972).
15. S. K. Lahiri, IBM Thomas J. Watson Research Center, Yorktown Heights, NY, private communication.
16. S. Basavaiah and S. K. Lahiri, *J. Appl. Phys.* **45,** 2773 (1974).

Received July 19, 1979; revised October 19, 1979

The authors are located at the IBM Zurich Research Laboratory, 8803 Rüschlikon, Switzerland.